Dust Environment and Dynamical History of a Sample of Short Period Comets

F.J. Pozuelos[1], F. Moreno[1], F. Aceituno[1], V. Casanova[1], A. Sota[1], J. Castellano[2], E. Reina[2], A. Diepvens[2], A. Betoret[2], B. Häusler[2], C. González[2], D. Rodríguez[2], E. Bryssinck[2], E. Cortés[2], F. García[2], F. García[2], F. Limón[2], F. Grau[2], F. Fratev[2], F. Baldrís[2], F. A. Rodriguez[2], F. Montalbán[2], F. Soldán[2], G. Muler[2], I. Almendros[2], J. Temprano[2], J. Bel[2], J. Sánchez[2], J. Lopesino[2], J. Báez[2], J. F. Hernández[2], J. L. Martín[2], J. M. Ruiz[2], J. R. Vidal[2], J. Gaitán[2], J. L. Salto[2], J. M. Aymamí[2], J. M. Bosch[2], J. A. Henríquez[2], J. J. Martín[2], J. Lacruz[2], L. Tremosa[2], L. Lahuerta[2], M. Reszelsky[2], M. Rodríguez[2], M. Camarasa[2], M. Campas[2], O. Canales[2], P.J. Dekelver[2], Q. Moreno[2], R. Benavides[2], R. Naves[2], R. Dymoc[2], R. García[2], S. Lahuerta[2], T. Climent[2]

[1] Instituto de Astrofísica de Andalucía (CSIC), Glorieta de la Astronomía s/n, 18008 Granada, Spain
e-mail: `pozuelos@iaa.es`

[2] Amateur Association Cometas-Obs, Spain

ABSTRACT

Aims. In this work we present an extended study of the relationship between the dust environment of a sample of short period comets and their dynamical history. To this end, we characterized the dust tails when the comets are active and we made a statistical study to determine their dynamical evolution. The targets selected were 22P/Kopff, 30P/Reinmuth 1, 78P/Gehrels 2, 115P/Maury, 118P/Shoemaker-Levy 4, 123P/West-Hartley, 157P/Tritton, 185/Petriew, and P/2011 W2 (Rinner).

Methods. We use two different observational data: a set of images taken in the Observatorio de Sierra Nevada, and the $Af\rho$ curves provided by the amateur astronomical association *Cometas-Obs*. In order to model these observations we use our Monte Carlo dust tail code. From this analysis we derive the dust parameters which best describe the dust environment: dust loss rates, ejection velocities and size distribution of particles. On the other hand, to study the dynamical

history of the comets we use a numerical integrator, which allow us to determine with a 90% of confidence level the time spent by these objects in the region of Jupiter Family Comets.

Results. From the Monte Carlo dust tail code, we characterized the dust environment of the referred objects, describing the dust mass loss rate, terminal velocities and size distributions as functions of the heliocentric distance for each target. The dynamical study points to a certain correlation between comet activity and time spent in the Jupiter Family region, although this trend is not always fulfilled.

Key words. comets: general – comets: short period comets – comets: dust environment – comets: dynamical history – methods: numerical integration

1. Introduction

According to the current theories, comets are the most volatile and least processed materials in our Solar System, which was formed from the primitive nebula 4.6 Gyr ago. They are considered as fundamental building blocks of giants planets and might be an important source of water on Earth (Hartogh et al. 2011). For these reasons comet research is a hot topic in science today, and quite a few spacecraft missions were devoted to their study; *Giotto* to the 1P/Halley (Keller et al. 1986), *Deep Space 1* to the 19P/Borrelly (Soderblom et al. 2002), *Stardust* to 81P/Wild 2 (Brownlee et al. 2004), *Deep Impact* to 9P/Temple 1 (A'Hearn et al. 2005) and the current Rosetta mission on its way to 67P/Churyumov-Gerasimenko (Schwehm & Schulz 1998) are some examples. It is well known the importance of the study of short periods comets, also called Jupiter Family Comets, because they offer the possibility to be studied during several passages near perihelion, when the activity increase, allowing to determine the dust environment and its evolution along the orbital path. This information is necessary to constraint the models describing evolution of different comet families and their contribution to the interplanetary dust (Sykes et al. 2004). In this work we focus on nine Jupiter Family Comets: 22P/Kopff, 30P/Reinmuth 1, 78P/Gehrels 2, 115P/Maury, 118P/Shoemaker-Levy 4, 123P/West-Hartley, 157P/Tritton, 185P/Petriew, and P/2011 W2 (Rinner) (hereafter 22P, 30P, 78P, 115P, 118P, 123P, 157P, 185P, and Rinner respectively). The perihelion distance, aphelion distance, orbital period, and lastest perihelion date are displayed in table 1. The analysis we have done consists in two different parts, the first one is a dust characterization using our Monte Carlo dust tail code, which was develop by Moreno (2009) and was used successfully on previous studies (e.g. Moreno et al. (2012), from which we adopt the results for comet 22P, see below). This procedure allow us to derive the dust parameters: mass loss rates, ejection velocities, and size distribution of particles (i.e. maximum size, minimum size and the power index of the distribution δ). We can also obtain information on the emission pattern, i.e., on the emission anisotropy. For the cases where we determine that the emission is anisotropic we can establish the location of the active areas on the surface and the rotational parameters as introduced by Sekanina (1981), i.e., the obliquity of the orbit plane to the cometary equator, I, and the argument of the sub-

Table 1. Targets list

Comet	q (AU)	Q (AU)	Period (yr)	Last perihelion date
22P	1.57	5.33	6.43	May 25, 2009
30P	1.88	5.66	7.34	April 19, 2010
78P	2.00	5.46	7.22	January 12, 2012
115P	2.03	6.46	8.76	October 6, 2011
118P	1.98	4.94	6.45	January 2, 2010
123P	2.12	5.59	7.59	July 4, 2011
157P	1.35	5.46	6.31	February 20, 2010
185P	0.93	5.26	5.46	August 13, 2012
Rinner	2.30	5.29	7.40	November 6, 2011
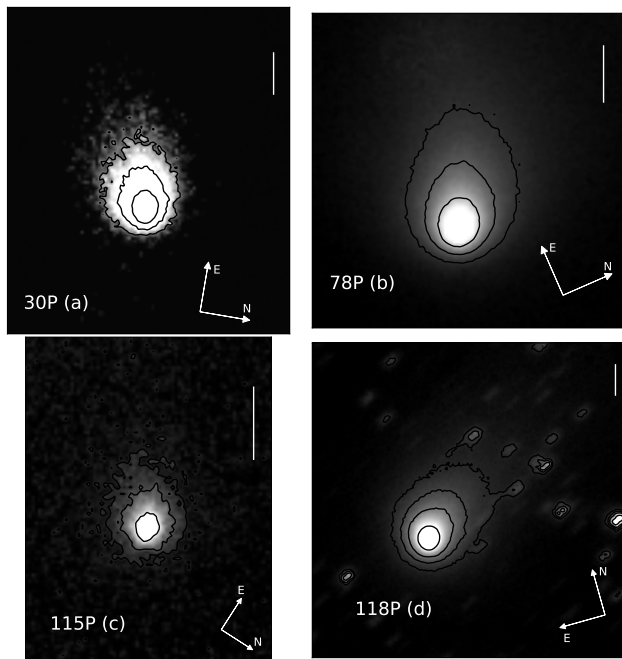
Fig. 1. Observations obtained using a CCD camera at 1.52 m telescope of the Observatorio de Sierra Nevada in Granada, Spain. (a) 30P/Reinmuth 1 on May 15, 2010. Isophote levels in Solar Disk Units (SDU) are: 2.00×10^{-13}, 0.75×10^{-13}, 0.25×10^{-13}. (b) 78P/Gehrels 2 on December 19, 2011. Isophote levels are: 0.55×10^{-12}, 2.65×10^{-13}, 1.35×10^{-13}. (c) 115P/Maury on July 15, 2011. Isophote levels are: 1.00×10^{-13}, 3.00×10^{-14}, 1.30×10^{-14}. (d) 118P/Shoemaker-Levy 4 on December 12, 2009. Isophote levels are: 1.50×10^{-13}, 6.00×10^{-14}, 3.50×10^{-14}, 2.00×10^{-14}. In all cases the directions of celestial North and East are given. The vertical bars correspond to 10^4 km in the sky.

solar meridian at perihelion, ϕ. The second part in our study is the analysis of the recent (15 Myr) dynamical history for each target. To perform this task we use the numerical integrator developed by Chambers (1999) as did by other authors before (e.g., Hsieh et al. 2012a,b; Lacerda 2013).This will serve to derive the time spent by each comet in each region, and specifically in the Jupiter Family region, where it is supposed that the comets become active periodically. For some of these comets, this is the first available study to our knowledge.

2. Observations and data reduction

The first block of our observation data were taken at the 1.52 m telescope of Sierra Nevada Observatory (OSN) in Granada, Spain. We used a 1024×1024 pixel CCD camera with a Johnson red filter. The pixel size in the sky was 0."46 so the field of view was 7'.8×7'.8. To improve the signal-
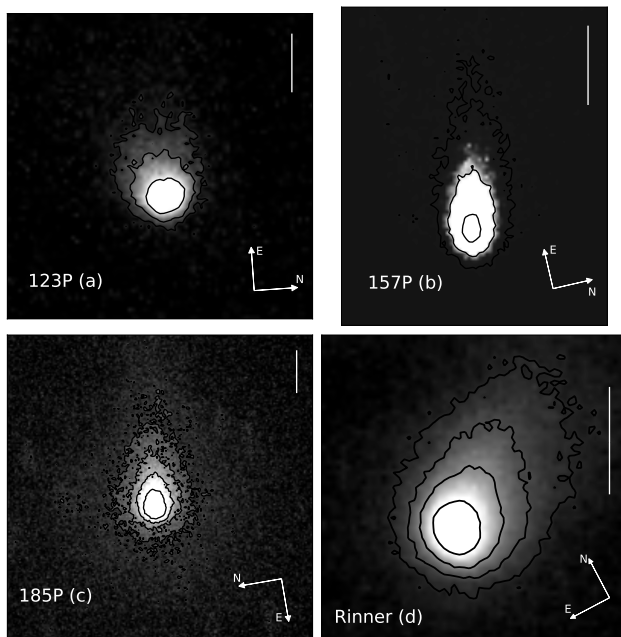
Fig. 2. Observations obtained using a CCD camera at 1.52 m telescope of the Observatorio de Sierra Nevada in Granada, Spain. (a) 123P/West-Hartley on February 26, 2011. Isophote levels in Solar Disk Units (SDU) are: 1.00×10^{-13}, 0.35×10^{-13}, 0.15×10^{-13}. (b) 157P/Tritton on March 10, 2010. Isophote levels are: 6.00×10^{-13}, 0.75×10^{-13}, 2.65×10^{-14}. (c) 185P/Petriew on July 15, 2012. Isophote levels are: 1.80×10^{-13}, 1.00×10^{-13}, 0.60×10^{-13}, 0.35×10^{-13}. (d) P/2011 W2 (Rinner) on January 4, 2012. Isophote levels are: 6.00×10^{-14}, 2.70×10^{-14}, 1.50×10^{-14}, 0.80×10^{-14}. In all cases the directions of celestial North and East are given. The vertical bars correspond to 10^4km in the sky.

to-noise ratio, the comets were imaged several times using integration times in the range 60-300 sec. The individual images at each night were bias subtracted and flat-fielded using standard techniques. The flux calibration was made using the USNO-B1.0 star catalog (Monet et al. 2003).The individual images of the comets were calibrated to mag arcsec^{-2} and then converted to solar disk intensity units (hereafter SDU). After calibration, the images corresponding to each single night were shifted to a reference image by taking into account their apparent sky motion, and then a median of those images was taken. For the modeling purposes, the final images are rotated to the photographic plane (N, M) (Finson & Probstein 1968) where the Sun is toward $-M$. Table 2 shows the log of the observations. Negative values in time to perihelion correspond to pre-perihelion observations. Representative images are displayed in Figs. 1 and 2.

The second block of observational data correspond to the $Af\rho$ curves around perihelion date ($\sim$ 300 days). These observations were carried out by the amateur astronomical association *Cometas-Obs*. The $Af\rho$ measurements are presented as a function of the heliocentric distance and are always referred to an aperture of radius $\rho = 10^4$ km projected on the sky at each observation date. The calibration of the *Cometas-Obs* observations was performed with the star catalogs CMC-14 and USNO A2.0.

3. Monte Carlo dust tail model

The dust tail analysis was performed by the Monte Carlo dust tail code which allows us to fit the OSN images, and the observational $Af\rho$ curves provided by *Cometas-Obs*. This code has been

Table 2. Log of the OSN observations

Comet	Observation Date (UT)	r_h [1] (AU)	Δ (AU)	Resolution (km pixel^{-1})	Phase Angle (°)	Position Angle (°)	$Af\rho$ ($\rho = 10^4 km$) [2] (cm)
30P/Reinmuth 1	2010 Mar 10 21:45	-1.916	1.579	526.8	31.1	87.1	52
	2010 May 15 21:10	1.898	2.147	716.3	28.0	99.6	61
78P/Gehrels 2	2011 Dec 19 20:00	-2.018	1.647	549.5	28.9	66.5	380
	2012 Jan 4 20:15	-2.009	1.805	602.2	29.2	67.0	470
115P/Maury	2011 Jul 2 22:00	-2.146	1.343	448.0	18.5	122.7	17
118P/Shoemaker-Levy 4	2009 Dec 12 01:45	-1.991	1.032	1377.2	8.9	324.9	103
123P/West-Hartley	2011 Feb 26 23:00	-2.346	1.970	657.3	24.5	86.4	40
	2011 Mar 31 21:00	2.253	2.252	751.3	25.6	85.4	50
157P/Tritton	2010 Mar 10 21:30	1.376	1.343	448.0	42.8	77.0	20
185P/Petriew	2012 Jul 15 03:15	-1.027	1.097	366.0	57.0	260.2	17
P/2011 W2 (Rinner)	2011 Dec 22 03:00	2.326	1.451	484.1	14.0	309.9	18
	2012 Jan 4 02:00	2.340	1.412	471.2	10.2	332.2	22

Notes.
[1] Negative values correspond with pre-perihelion, positive values with post-perihelion.
[2] The $Af\rho$ values for phase angle $\leq 30°$ have been corrected according to the equation (2) (see text).

successfully used on previous works on characterization of dust environments of comets and Main-belt comets, such as 29P/Schwassmann-Wachmann 1 and P/2010 R2 (La Sagra) (Moreno 2009; Moreno et al. 2011). This code is also called the Granada model (see Fulle et al. 2010) in the dust studies for the Rosetta mission target, 67P/Churyumov-Gerasimenko. The model describes the motion of the particles when they leave the nucleus and are submitted to the gravity force of the Sun and the radiation pressure, so that the trajectory of the particles around the Sun is Keplerian. The β parameter is defined as the ratio of the radiation pressure force to the gravity force, and is given for spherical particles, as $\beta = C_{pr}Q_{pr}/(\rho_d d)$, where $C_{pr} = 1.19 \times 10^{-3}$ km m^{-2}, Q_{pr} is the scattering efficiency for radiation pressure, which is $Q_{pr} \sim 1$ for large absorbing grains (Burns et al. 1979), ρ_d is the mass density, assumed at $\rho_d = 10^3$ kg m^{-3}, and d is the particle diameter. We use Mie theory for the interaction of the electromagnetic field with the spherical particles to compute the geometric albedo, p_v, and Q_{pr}. p_v is a function of the phase angle α and the particle radius. We assume the particles as glassy carbon spheres of refractive index $m = 1.88 + 0.71i$ (Edoh 1983) at $\lambda = 0.6$ μm. We compute a large number of dust particle trayectories and calculate their positions on the (N, M) plane, and their contribution to the tail brightness. The free parameters of the model are dust mass lost rate, the ejection velocities of the particles, the size distribution, and the dust ejection pattern.

3.1. $Af\rho$

The $Af\rho$ quantity [cm] (A'Hearn et al. 1984) is related to the dust coma brightness where A is the dust geometric albedo, f the filling factor in the aperture field of view (proportional to the dust optical thickness), and ρ is the linear radius of aperture at the comet, i.e., the sky-plane radius. When the cometary coma is in steady-state, $Af\rho$ is independent of the observation coma radius ρ

if the surface brightness of the dust coma is proportional to ρ^{-1}. It is formulated as follows:

$$Af\rho = \frac{4r_h^2\Delta^2}{\rho}\frac{F_c}{F_s} \tag{1}$$

where r_h is the heliocentric distance, and Δ the geocentric distance. F_c is the measured cometary flux integrated within a radius of aperture ρ, and F_s is the total solar flux. For each comet we have the $Af\rho$ curve as heliocentric distance function provided by *Cometas-Obs*, for an aperture of radius $\rho = 10^4$ km, $\sim$ 300 days around perihelion, and the $Af\rho$ measurements derived from the OSN observations with the same aperture. Some of the $Af\rho$ data correspond to times where the phase angle was close to zero degree, so that the backscattering enhancement because apparent (Kolokolova et al. 2004). We could not model this enhancement, because for the assumed abosrbing spherical particles, the phase function is approximately constant except for the forward spike, for particles whose radius is r$\geq$ λ. Then, we corrected these enlarged $Af\rho$ at small phase angles by assuming a certain linear phase coefficient wich we apply to the data at phase angles $\alpha \leq 30°$. We adopted a linear phase coefficient of 0.03 mag deg^{-1}, which is in the range 0.02-0.04 mag deg^{-1} estimated by Meech & Jewitt (1987) from varius comets. In this way, the corrected $Af\rho'$ values are computed as a function of the original $Af\rho$ values at phase angle α as:

$$Af\rho' = 10^{\frac{-\beta(30-\alpha)}{2.5}}Af\rho \tag{2}$$

To ilustrate this correction, we show in Fig. 3 its application to comet 78P/Gehrels 2. In the upper panel it is seen the correlation of the original $Af\rho$ data with the phase angle, and the lower panel the final $Af\rho$ curve after correction those values by equation (2). The same equation is applied to the OSN images when the phase angle is $\alpha \leq 30°$ (see table 2).

4. Dust analysis

As described in the previous section, we use our Monte Carlo dust tail code to retrieve the dust properties of each comet in our sample. The code has many important parameters, so that a number of simplifying assumptions should be made in order to make the problem tractable. The dust particles are assumed spherical, with a density of 1000 kg m^{-3} and a refractive index of $m = 1.88+0.71i$, which is typical of carbonaceous spheres at red wavelengths (Edoh 1983). This gives a geometric albedo of $p_v = 0.04$ for particles sizes of r$\gtrsim$ 1μm at a wide range of phase angles. The particle ejection velocity is parametrized as $v(t,\beta) = v_1(t) \times \beta^{1/2}$ where $v_1(t)$ is a time dependent function to be determined in the modeling procedure. In addition, the emission pattern, i.e., possible spatial asymmetries in the particle ejection might appear. The asymmetric ejection pattern is parametrized by considering a rotating nucleus with active areas on it, whose rotating axis is defined by the inclination, I, and the argument of the subsolar meridian at perihelion, as defined in Sekanina (1981). The rotation period, P, is not generally constrained if the ejecta age is much longer than P, which is normally the case. The particles will be assumed distributed broadly in size, so that the minimum
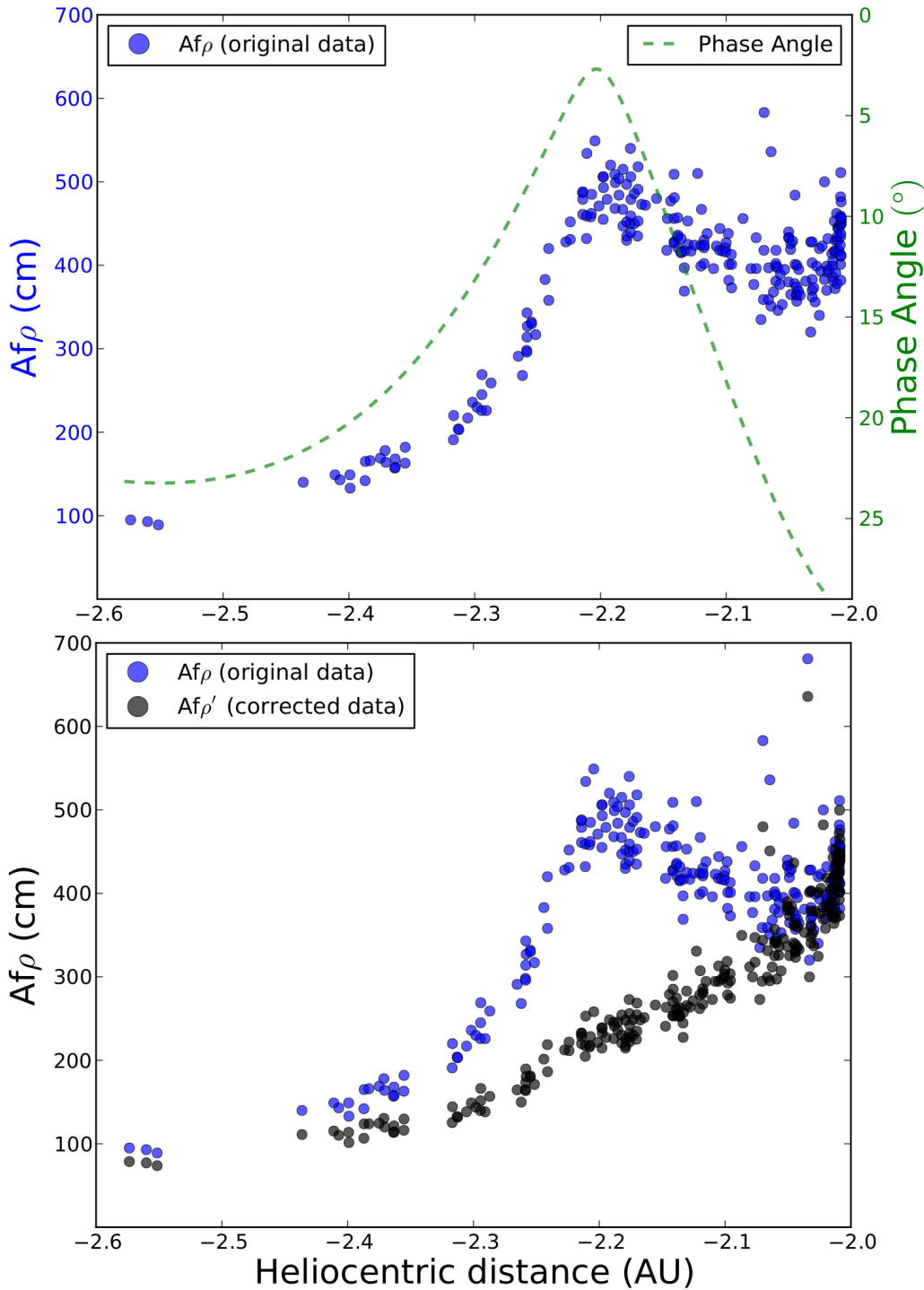
Fig. 3. $Af\rho$ pre-perihelion measurements of comet 78P/Gehrels 2 provided by *Cometas-Obs*. Upper panel: original $Af\rho$ measurements and phase angle as function of heliocentric distance. Lower panel: $Af\rho$ and $Af\rho'$ after the backscattering effect correction using equation (2) as function of heliocentric distance.

size is always set in principle in the sub-micrometer range, while the maximum size is set in the centimetre range. The size distribution is assumed to be given by a power law, $n(r) \propto r^{-\delta}$, where δ is set to vary in the -4.2 to -3 domain which is the range that has been determined for other comets (e.g., Jockers 1997). All of those parameters, $v(t)_1$, r_{min}, r_{max}, δ, and the mass loss rate are function of the heliocentric distance, so that some kind of dependence on r_h must be established. In addition,

the activity onset time should also be specified. On the other hand, current knowledge of physical properties of cometary nuclei established the bulk density below $\rho = 1000$ kg m^{-3} (Carry 2012). Values of $\rho = 600$ kg m^{-3} have been reported for comets 81P/Wild 2 (Davidsson & Gutierrez 2004) and Temple 1 (A'Hearn et al. 2005), so we adopted that value. The ejection velocity at a distance R$\sim 20R_N$, where R$_N$ is the nucleus radii and R the distance where the gas drag vanishes, should overcome the escape velocity, which is given by $v_{esc} = \sqrt{2GM/R}$. Assuming a spherically-shaped nucleus, we get $v_{esc} = R_N \sqrt{(2/15)\pi\rho G}$, where $\rho = 600$ kg m^{-3}. In cases where R_N has been estimated by other authors, the minimum ejection velocity should verify the condition $v_{min} \gtrsim v_{esc}$. In all the other cases, considering that the minimum particle velocity determined in the model is $v_{min} \sim v_{esc}$, we can give an upper limit estimate of the nucleus radius.

The Monte Carlo dust tail code is a forward code whose output is a dust tail image corresponding to a given set of input parameters. Given the large amount of parameters, the solution is likely not unique: approximately the same tail brightness can be likely achieved by assuming another set of input parameters. However, if the number of available images and/or $Af\rho$ measurements cover a significant orbital arc, it is clear that the indetermination is reduced. Our general procedure consists first in assuming the most simple case: isotropic particle ejection, $r_{min} = 1\mu$m, $r_{max} = 1$cm, $v_1(t)$ monotonically increasing toward perihelion, $\delta = -3.5$, and dM/dt set to a value which reproduce the measured tail intensity in the optocenter, assuming a monotonic decrease with heliocentric distance. From this starting point, we then start to vary the parameters, assuming certain different dependency with heliocentric distance, until an acceptable agreement with both the dust tail images and the $Af\rho$ measurements is reached. Then, if after many trial-and-error procedures we find no way to fit the data using an isotropic ejection model, we switch to the anisotropic model where the active area location and rotational parameters must be set.

Using the procedure described above for each comet in the sample, we present the results on the dust parameters organized in the following way: in tabular form, where the main properties of the dust environment of each comet is given (tables 3 and 4) , and a series of plots on the dependence on the heliocentric distance of the dust mass loss rate, the ejection velocities for $r = 1$ cm particles, the maximum particle size, and the power index of the size distribution (figures from 4 to 11). In addition, the fits to the isophote fields of the available images and to the measured $Af\rho$ values by *Comets-Obs*, are also displayed for each target (figures from 12 to 19).
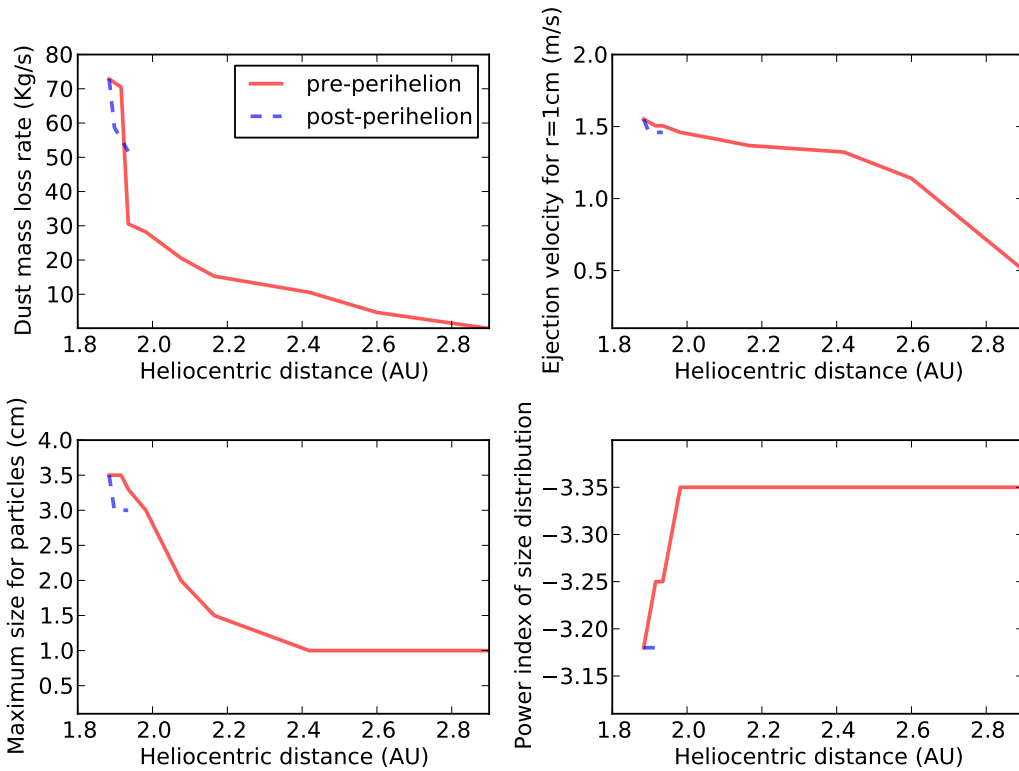
Fig. 4. 30P dust characterization. The panels correspond with the dust parameters obtained in the model which are function of the heliocentric distance. (a) Dust mass loss rate [kg/s]; (b) Ejection velocities for particles of r=1 cm glassy carbon spheres [m/s]; (c) Maximum size of the particles [cm]; and (d) power index of the size distribution. In all cases the solid red-line corresponds to pre-perihelion and the dashed blue-line with post-perihelion.

4.1. Discussion

The dust characterization of the 22P was already reported by Moreno et al. (2012), where the authors concluded that this comet shows a clear time dependent asymmetric ejection behavior, with an enhanced activity at heliocentric distances beyond 2.5 AU pre-perihelion, also accompanied by enhanced particle ejection velocity. The maximum size for the particles were estimated as 1.4 cm with a constant power index of -3.1. The peak of dust mass loss rate, and the peak of ejection velocities were reached at perihelion with values $Q_d = 260$ kg s^{-1} and $v = 2.7$ m s^{-1} for 1-cm grains. The total dust lost per orbit was 8×10^9 kg. The annual dust loss rate is $T_d = 1.24 \times 10^9$ kg yr^{-1} , and the averaged dust mass loss rate per orbit is 40 kg/s. The contribution to the interplanetary dust of this comet corresponds to about 0.4% of the $\sim 2.9 \times 10^{11}$ kg yr^{-1} that must be replenished if the cloud of interplanetary dust is in steady state (Grun et al. 1985).

For 30P, 115P, and 157P we derived an anisotropic ejection pattern with active areas on the nucleus surface (see table 3). In the case of 30P, the rotational parameters i.e. I and ϕ, have been taken from Krolikowska et al. (1998) as $I = 107°$ and $\phi = 321°$. However, for 115P and 157P these parameters have been derived from the model. The 78P is the most active comet in our sample, with
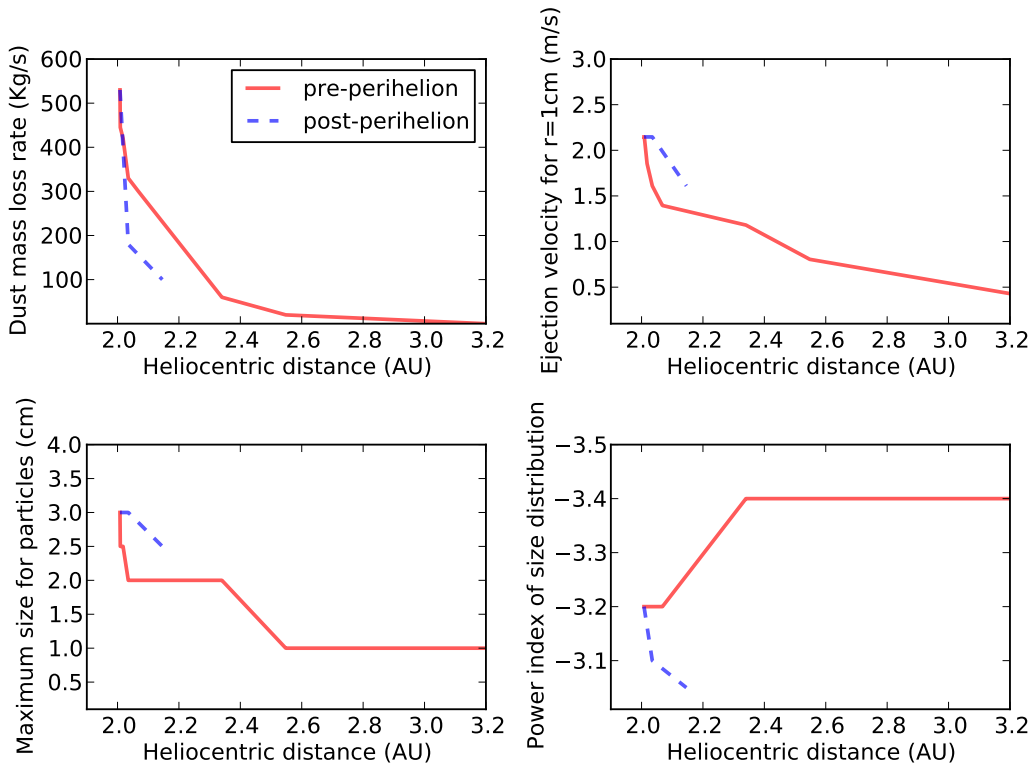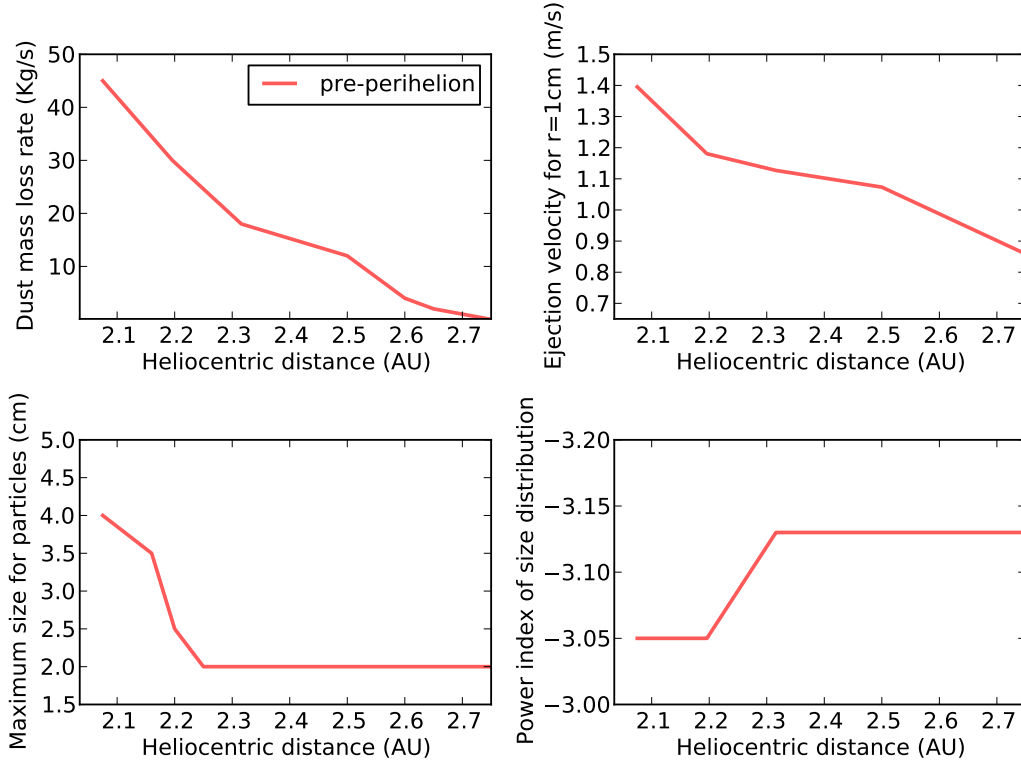
Fig. 5. 78P dust characterization. The panels correspond with the dust parameters obtained in the model which are heliocentric distance function. (a) Dust mass loss rate [kg/s]; (b) Ejection velocities for particles of r=1 cm glassy carbon spheres [m/s]; (c) Maximum size of the particles [cm]; and (d) power index of the size distribution. In all cases the solid red-line corresponds to pre-perihelion and the dashed blue-line with post-perihelion.
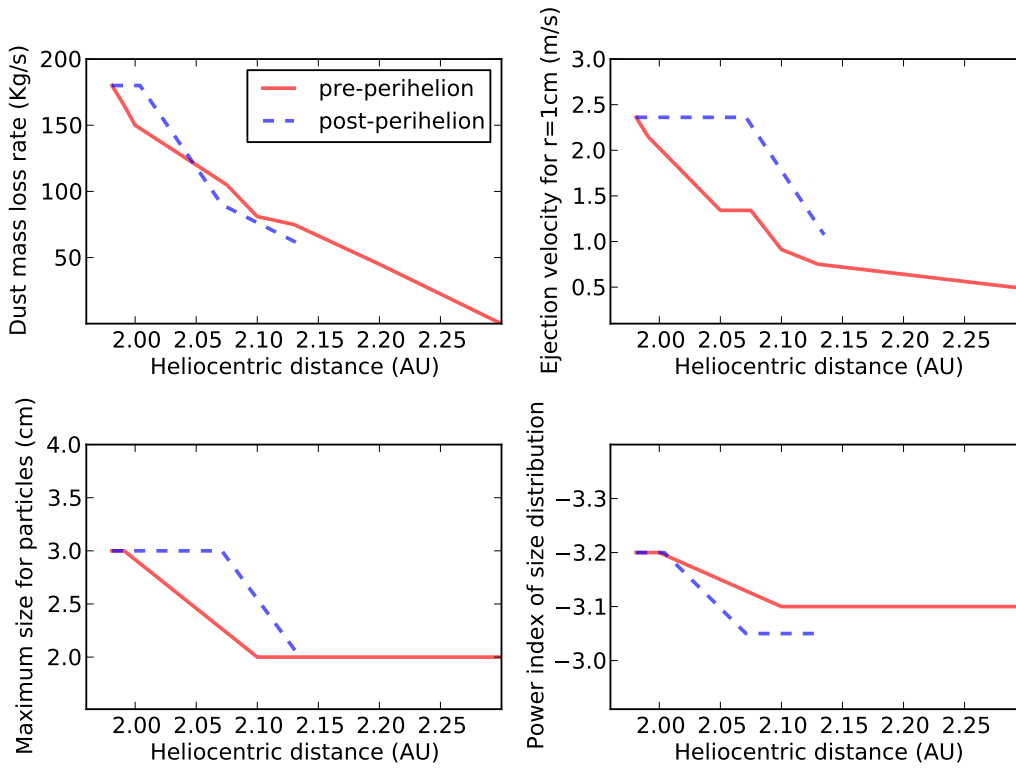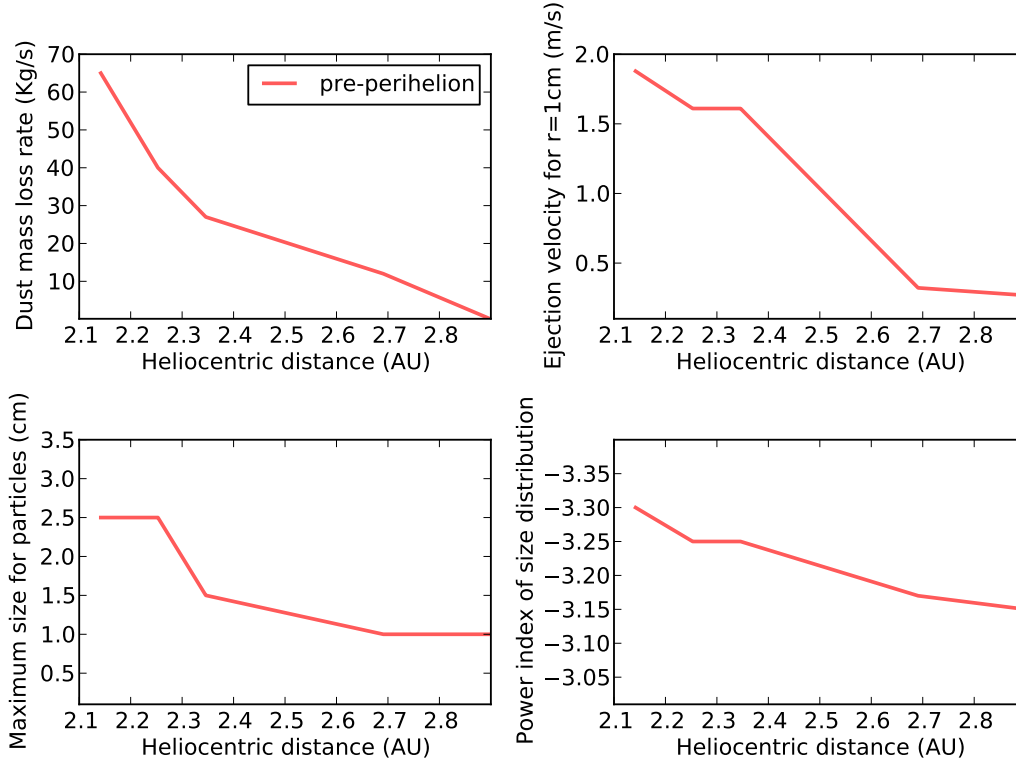

Fig. 6. 115P dust characterization. The panels correspond with the dust parameters obtained in the model which are heliocentric distance function. (a) Dust mass loss rate [kg/s]; (b) Ejection velocities for particles of r=1 cm glassy carbon spheres [m/s]; (c) Maximum size of the particles [cm]; and (d) power index of the size distribution. In all cases the solid red-line corresponds to pre-perihelion.

Fig. 7. 118P dust characterization. The panels correspond with the dust parameters obtained in the model which are heliocentric distance function. (a) Dust mass loss rate [kg/s]; (b) Ejection velocities for particles of r=1 cm glassy carbon spheres [m/s]; (c) Maximum size of the particles [cm]; and (d) power index of the size distribution. In all cases the solid red-line corresponds to pre-perihelion and the dashed blue-line with post-perihelion.
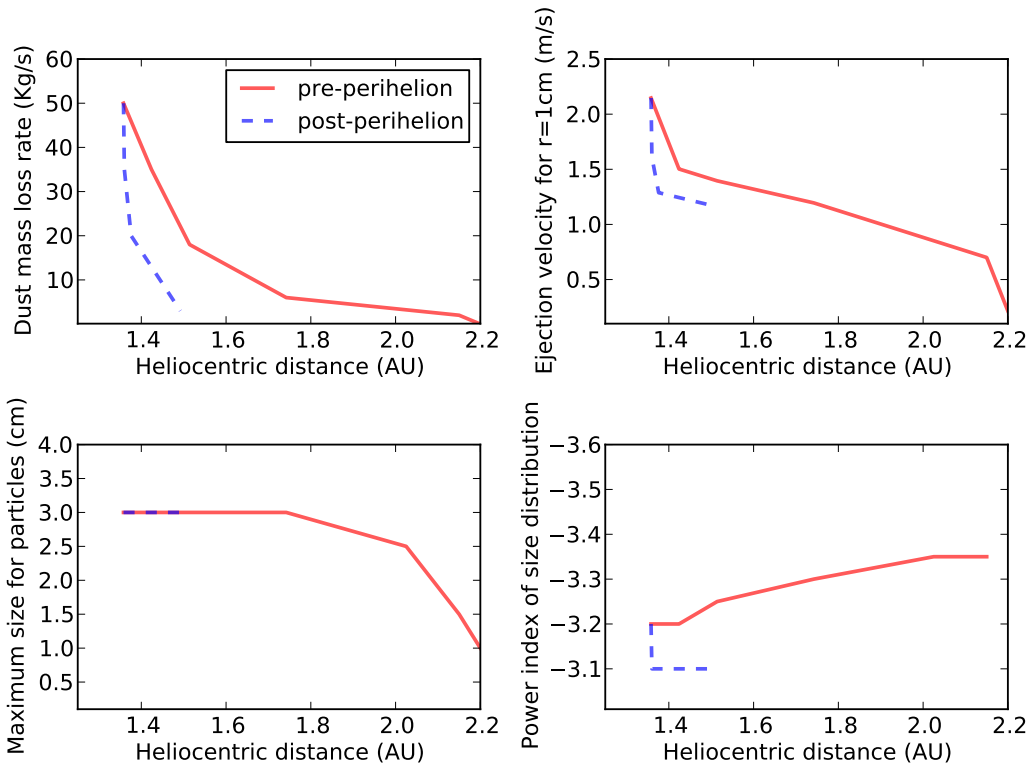

Fig. 8. 123P dust characterization. The panels correspond with the dust parameters obtained in the model which are heliocentric distance function. (a) Dust mass loss rate [kg/s]; (b) Ejection velocities for particles of r=1 cm glassy carbon spheres [m/s]; (c) Maximum size of the particles [cm]; and (d) power index of the size distribution. In all cases the solid red-line corresponds to pre-perihelion.

Fig. 9. 157P dust characterization. The panels correspond with the dust parameters obtained in the model which are heliocentric distance function. (a) Dust mass loss rate [kg/s]; (b) Ejection velocities for particles of r=1 cm glassy carbon spheres [m/s]; (c) Maximum size of the particles [cm]; and (d) power index of the size distribution. In all cases the solid red-line corresponds to pre-perihelion and the dashed blue-line with post-perihelion.

a peak dust loss rate at perihelion with a value of $Q_d = 530$ kg s^{-1} and a total dust mass ejected of 5.8×10^9 kg. This comet was study by Mazzotta Epifani & Palumbo (2011) in its previous perihelion passage on October 2004. The authors estimated the dust production rate at perihelion with values between $Q_d = 14 - 345$ kg s^{-1}, using a method derived from the one used by Jewitt (2009) to compute the dust production rate of active Centarus. They also obtained $Af\rho = 846 \pm 55$ cm in an aperture of radius $\rho = 7.3 \times 10^3$ km and they concluded that this comet is more active the the average Jupiter Family Comets at a given heliocentric distance. In addition, Lowry & Weissman (2003) reported a stellar appearance of 78P at $r_h = 5.46$ AU pre-perihelion, and any possible coma contribution to the observed flux was likely to be small or non existent, which is consistent with our model, where the comet is not active at such large pre-perihelion distances. From our studies we can classify our targets in three different categories: weakly active comets (115P, 157P, and Rinner), with an average annual dust production rate of $T_d < 1 \times 10^8$ kg yr^{-1}, moderately active comets (30P, 123P, and 185P), with $T_d = 1 - 3 \times 10^8$ kg yr^{-1}, and highly active comets (22P, 78P, and 118P), for which $T_d > 8 \times 10^8$ kg yr^{-1}. It is necessary to take into account that for the comet 115P and 123P, we do not have observations after perihelion, i.e., our observational information covers less than half of the orbit, losing the part of the branch which is supposed to be the most active. For this reason our results for these comets are lower limits in the T_d measurements.
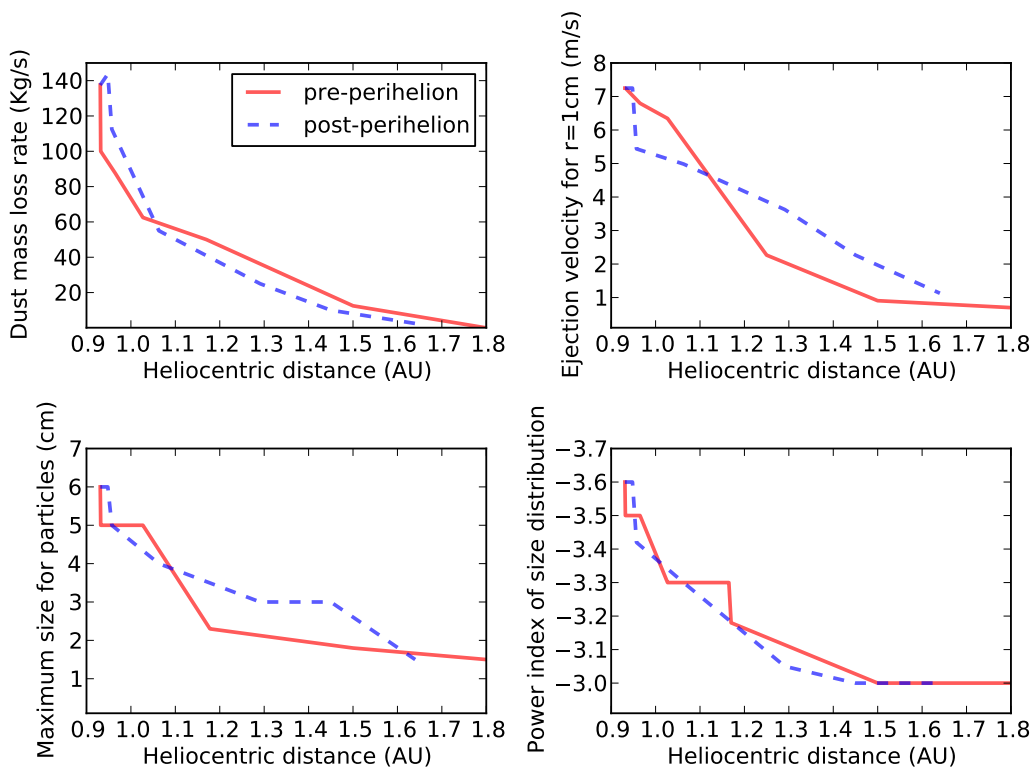
Fig. 10. 185P dust characterization. The panels correspond with the dust parameters obtained in the model which are heliocentric distance function. (a) Dust mass loss rate [kg/s]; (b) Ejection velocities for particles of r=1 cm glassy carbon spheres [m/s]; (c) Maximum size of the particles [cm]; and (d) power index of the size distribution. In all cases the solid red-line corresponds to pre-perihelion and the dashed blue-line with post-perihelion.

5. Dynamical history analysis

Levison & Duncan (1994) were the first to make a comprehensive set of long-term integrations (up to 10^7 yr) in order to study the dynamical evolution of short period comets. The authors argue that due to the chaotic nature of each individual orbit, it is necessary to make a statistical study using several orbits for each comet with slightly different initial orbital elements. For this reason the authors made a 10 Myr backward (and forward) integration for the 160 Short Period Comets know at that time, plus 3 clones for each comet with offsets in the positions along the x, y, and z directions of +0.01 AU, i.e. they used 640 test particles for their integrations. They conclude that the long-term integrations into the the past or future are statistically equivalent and they obtained that ~ 92% of the total particles were ejected from the Solar System and ~ 6% were destroyed by becoming Sungrazers. The median lifetime of Jupiter Family Comets (hereafter JFCs) was derived as 3.25×10^5 yr (Duncan et al. 2004). In our case, to determine the dynamical evolution of our targets, we use the Mercury package version 6.2, a numerical integrator developed by Chambers (1999), that has been used by other authors with the same purpose (e.g., Hsieh et al. 2012a,b; Lacerda 2013). Due to the chaotic nature of the targets, which was mentioned in the Levison & Duncan (1994) study, we generate a total of 99 clones having 2σ dispersion in three of the orbital elements: semimajor axis, eccentricity, and inclination (hereafter a, e, and i), where σ is the uncertainty in the corresponding parameter as given in the JPL Horizons on-line Solar System data (see ssd.pjl.nasa.gov/?horizons).
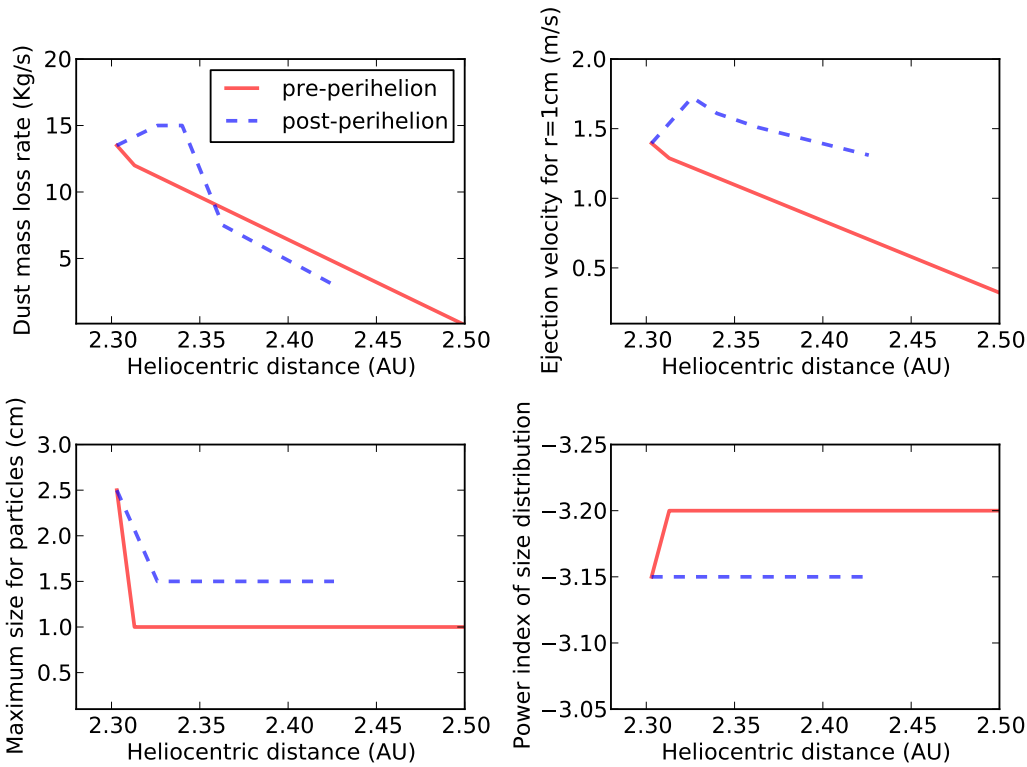
Fig. 11. Rinner dust characterization. The panels correspond with the dust parameters obtained in the model which are heliocentric distance function. (a) Dust mass loss rate [kg/s]; (b) Ejection velocities for particles of r=1 cm glassy carbon spheres [m/s]; (c) Maximum size of the particles [cm]; and (d) power index of the size distribution. In all cases the solid red-line corresponds to pre-perihelion and the dashed blue-line with post-perihelion.

In table 5 we show the orbital parameters and the 1σ uncertainty of our targets extracted from that web page. These 99 clones plus the real object make a total of 100 massless test particles in order to perform an statistical study for each comet, what suppose 900 massless test particles. The Sun and the eight planets are taken into account as massive bodies. We used the hybrid algorithm which combines a second-order mixed-variable symplectic algorithm with a Burlisch-Stoer integrator to control close encounters. The initial time step is 8 days, and the clones are removed any time during the integration when they are beyond 1000 AU from the Sun. The total integration time was 15 Myr, time enough to determine which are the most visited regions for each comet, and derive the time spent in the region of JFCs, region which is supposed to be the location where the comets reach temperature high enough to be active periodically. We divide the possible locations of the comets in four regions attending to their dynamical properties at each moment in the study: JFCs-type, with $a < a_S/(1 + e)$, Centaur-type, confined by $a_S/(1 + e) < a < a_N$ and $e < 0.8$, Halley-type, similar to Centaur-type but with $e > 0.8$, and Transneptunian-type, with $a > a_N$, where a_S and a_N are the semimajor axes of Saturn and Neptune, respectively.

In this study we neglect the non-gravitational forces using the same arguments as Lacerda (2013). Thus, assuming that the non-gravitational acceleration, T, is due to a single sublimation jet tangential to the comet orbit, the change rate of the semimajor axis is described by:
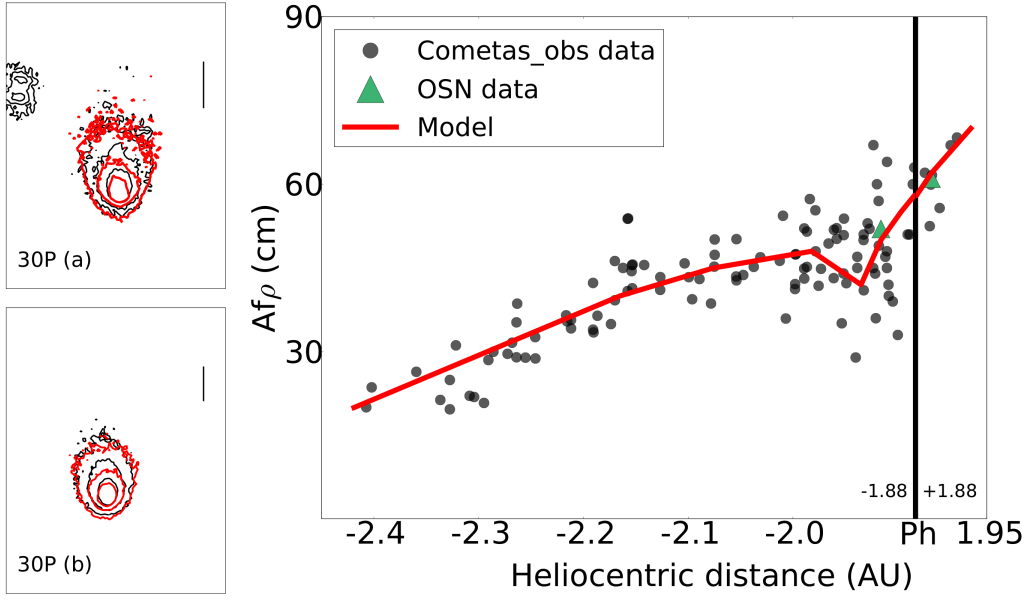
Fig. 12. 30P model fit. Isophote fields: (a) March 10, 2010, and (b) May 15, 2010. In both cases isophote levels are 2.00×10^{-13}, 0.75×10^{-13}, 0.25×10^{-13} SDU. The black contours correspond to the OSN observations, and the red contours to the model. Vertical bars correspond to 10^4 km on the sky. $Af\rho$ curve: The black dots correspond to Cometas-Obs data and the red line with the model. The green triangles are the OSN data which correspond to the March 10, 2010, and May 15, 2010. $\rho = 10^4$ km.
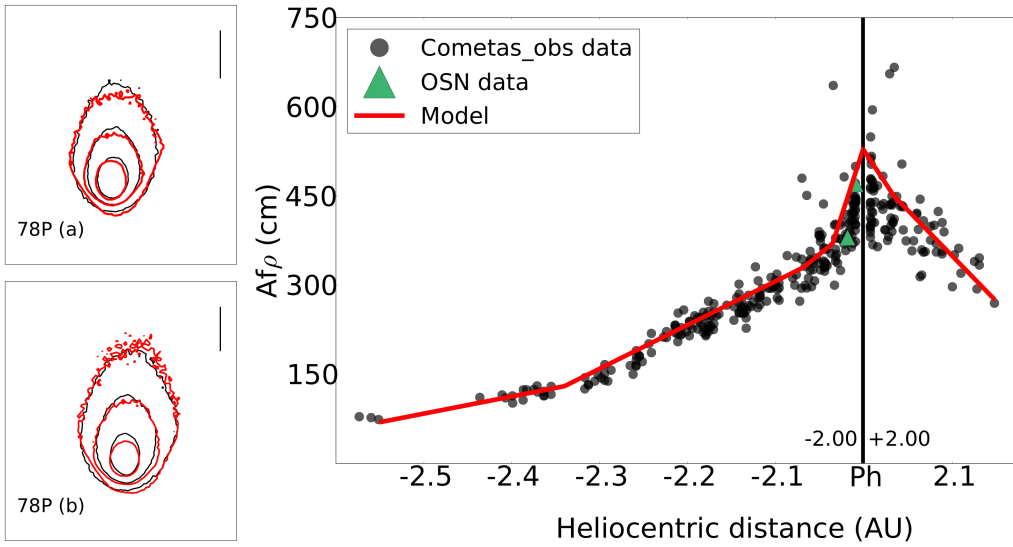
Fig. 13. 78P model fit. Isophote fields: (a) December 19, 2011, and (b) January 4, 2012. In all cases the isophote are 0.55×10^{-12}, 2.65×10^{-13}, and 1.35×10^{-13} SDU. The black contours correspond to the OSN observations, and the red contours to the model. Vertical bars correspond to 10^4 km on the sky. $Af\rho$ curve: The black dots correspond to Cometas-Obs data (corrected by equation (2) when phase angle $\alpha \leq 30°$) and the red line with the the model. The green triangles are the OSN data which correspond to December 19, 2011 and January 4, 5, and 6, 2012. $\rho = 10^4$ km.

$$da/dt = 2Va^2T/GM_\odot \qquad (3)$$

where T is the acceleration due to the single jet, given by:
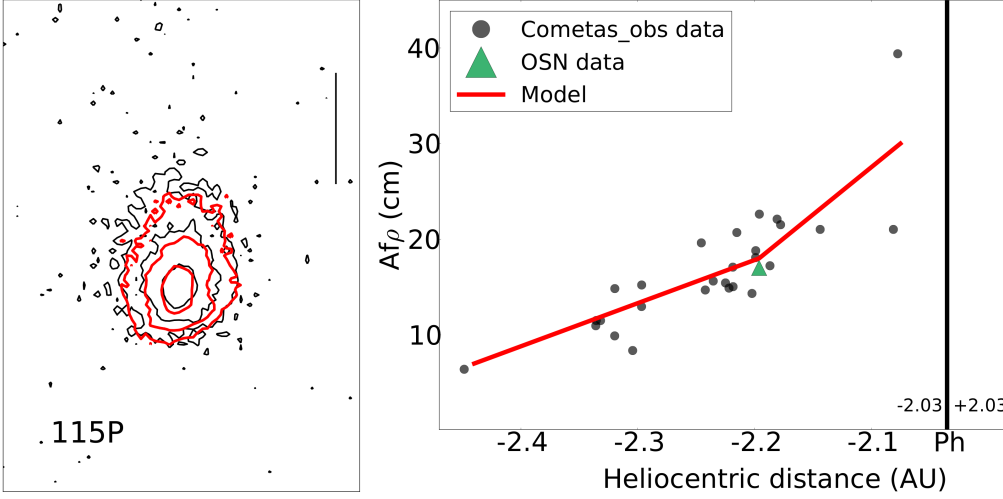
$$T = (dM_d/dt)(v_d/m_{nuc}) \qquad (4)$$

Fig. 14. 115P model fit. Isophote fields: July 15, 2011. Isophote levels are 1.00×10^{-13}, 3.00×10^{-14}, and 1.30×10^{-14} SDU. The black contours correspond to the OSN observations, and the red contours to the model. Vertical bar correspond to 10^4 km on the sky. Afρ curve: The black dots correspond to Cometas-Obs data (corrected by equation (2) when phase angle $\alpha \leq 30°$) and the red line with the model. The green triangle is the OSN datum which correspond to the July 15, 2011. $\rho = 10^4$ km.

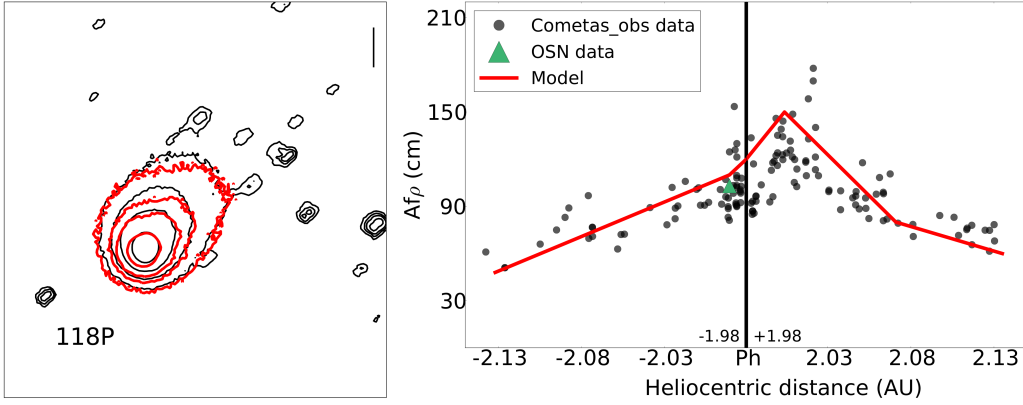**Fig. 15.** 118P model fit. Isophote fields: December 12, 2009. Isophote levels are 1.50×10^{-13}, 6.00×10^{-14} 3.50×10^{-14}, and 2.00×10^{-14} SDU. The black contours correspond to the OSN observations, and the red contours to the model. Vertical bar correspond to 10^4 km on the sky. Afρ curve: The black dots correspond to Cometas-Obs data (corrected by equation (2) when phase angle $\alpha \leq 30°$) and the red line with the model. The green triangle is the OSN datum which correspond to the December 12, 2009. $\rho = 10^4$ km.

In these equations, V is the orbital velocity, a is the semimajor axis, G is the gravitational constant, $M_\odot$ is the Sun mass, v_d is the dust velocity, and m_{nuc} is the mass of the nucleus. In order to show a general justification to neglect the gravitational forces valid to our complete list of targets, we compute the maximum rate of change of the semimajor axis will correspond to the comet using the maximum a, maximum dM/dt, maximum v_d, and minimum m_{nuc}. From our comet sample, these values are $a_{max} = 4.25$ AU (115P), $(dM/dt)_{max} = 47.5$ kg s^{-1} (78P), $(v_d)_{max} = 708$ m s^{-1} (185P). The minimum comet nucleus was inferred for 157P as $R_N \leq 1.6$ km, so we adopt $(m_{nuc})_{min} = 1.6$ km. Taken all those values together, we get $T = 2.2 \times 10^{-5}$ AU yr^{-2}, and $da/dt = 4.8 \times 10^{-5}$ AU yr^{-2}. On the other hand, the lifetime of sublimation from a single jet would be $t_{sub} = 4550$ yr, based on the nucleus size and $(dM/dt)_{max}$. Then, the total deviation in semimajor axis would be $(da/dt)_{max} \times t_{sub} = 0.21$ AU. This deviation, which should be considered as an
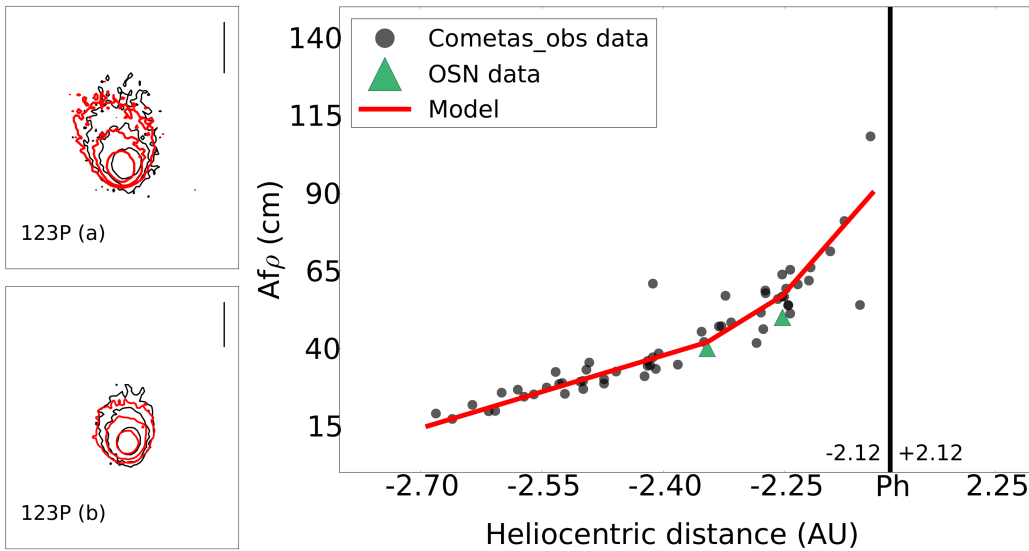
Fig. 16. 123P Isophote fields: (a) February 26, 2011 , and (b) March 31, 2011. Isophote levels are 1.00×10^{-13}, 0.35×10^{-13}, 0.15×10^{-13} SDU in (a) and 1.50×10^{-13}, 0.50×10^{-13}, 0.25×10^{-13} SDU in (b). The black contours correspond to the OSN observations, and the red contours to the model. Vertical bars correspond to 10^4 km on the sky. Afρ curve. The black dots correspond to Cometas-Obs data (corrected by equation (2) when phase angle $\alpha \leq 30°$) and the red line with the model. The green triangles are the OSN data which correspond February 26 and March 31 of 2011. $\rho = 10^4$km.

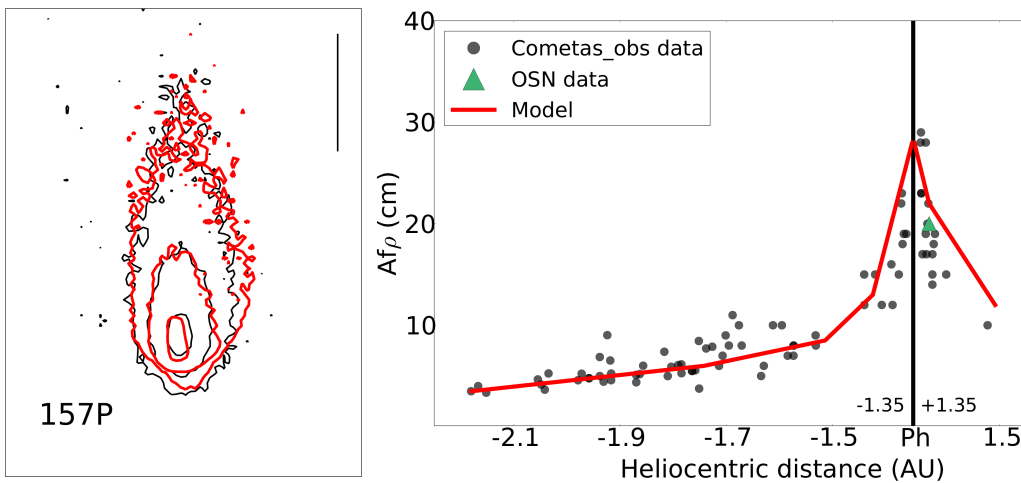**Fig. 17.** 157P model fit. Isophote fields: March 10, 2010. Isophote levels are 6.00×10^{-13}, 0.75×10^{-13}, and 2.65×10^{-14} SDU. The black contours correspond to the OSN observations, and the red contours to the model. Vertical bar correspond to 10^4 km on the sky. Afρ curve: The black dots correspond to Cometas-Obs data (corrected by equation (2) when phase angle $\alpha \leq 30°$) and the red line with the model. The green triangle is the OSN datum which correspond March 10, 2010. $\rho = 10^4$km.

upper limit, is completely negligible in the scale of variations we are dealing with in the dynamical analysis of the orbital evolution. This result is close to the one derived for Lacerda (2013), where the author gives the maximum semimajor deviation for P/2010 T020 LINEAR-Grauer as 0.42 AU.

As a result of our 15 Myr backward integration for all targets, we obtain that the ~ 98% of the particles are ejected before the end of the integration, and in almost all cases the surviving clones are in the transneptunian region. Thus, we focussed on the first 1 Myr of backward in the orbital evolution, where the ~ 20% of the test particles still remain in the Solar System. This time is enough to obtain a general view of the visited regions by each comet. After that we display the
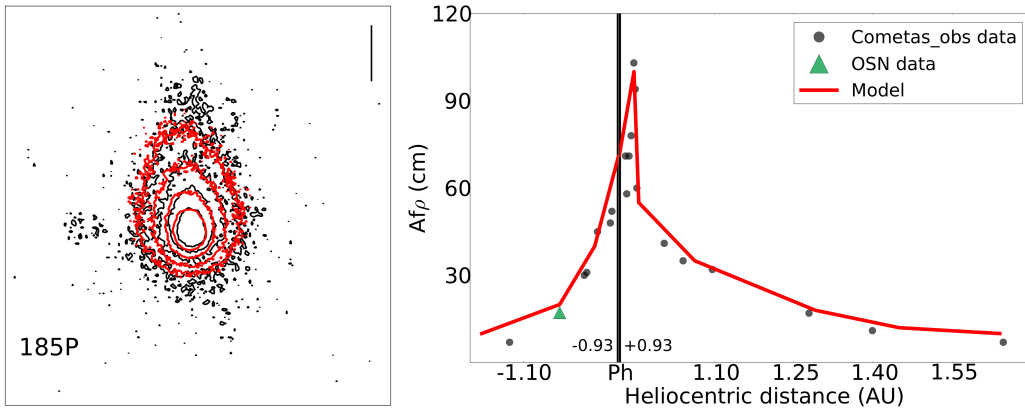
Fig. 18. 185P Isophote fields: July 15, 2012. Isophote levels are 1.80×10^{-13}, 1.00×10^{-13} 0.60×10^{-13}, and 0.35×10^{-13} SDU. The black contours correspond to the OSN observations, and the red contours to the model. Vertical bar correspond to 10^4 km on the sky. Afρ curve: The black dots correspond to Cometas-Obs data (corrected by equation (2) when phase angle $\alpha \leq 30°$) and the red line with the model. The green triangle is the OSN datum which correspond July 15, 2012. $\rho = 10^4$km.

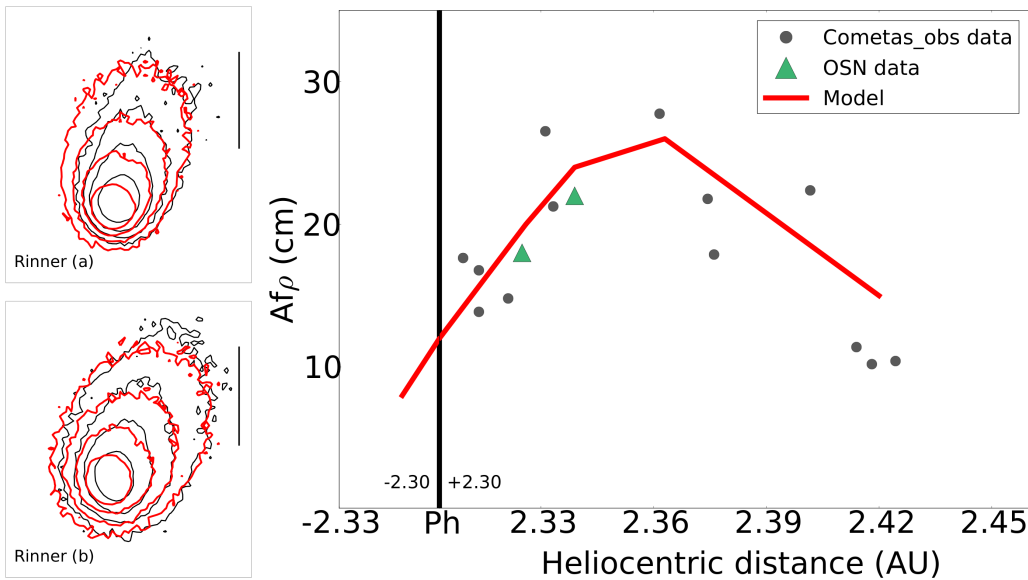**Fig. 19.** Rinner model fit. Isophote fields: (a) December 22, 2011. (b) January 4. In both cases the isophote are 6.00×10^{-14}, 2.70×10^{-14}, 1.50×10^{-14}, 0.80×10^{-14} SDU. The black contours correspond to the OSN observations, and the red contours to the model. Vertical bars correspond to 10^4 km on the sky. Afρ curve: The black dots correspond to Cometas-Obs data (corrected by equation (2) when phase angle $\alpha \leq 30°$) and the red line with the model. The green triangles are the OSN data which correspond with December 19, 2011 and January 4, 2012. $\rho = 10^4$km.

last 5000 yr with a 100 yr temporal resolution, in order to obtain the time spent by these comets in the JFCs region with a confidence level of 90%.

As an example of this procedure, we show in detail the results for 30P (see Fig. **?**) . For this comet we determined that 85% of the particles were ejected from the Solar System after 1 Myr of backward integration. We can see that most of the particles stay in the JFCs region during the first $\sim 2 \times 10^4$ yr , but at $\sim 2 \times 10^5$ yr they moved on into further regions as centaurs and transneptunian objects. To determine the time spent by 30P in JFCs region we show in Fig. 21 the last 5×10^3 yr with a resolution of 100 yr. We derive with 90% of confidence level, that 30P comet spent $\sim 2 \times 10^3$ yr in this location.

Table 5. Orbital parameters of the short period comets under study

Comet	e	a (AU)	i (°)	node (°)	peri (°)	M (°)
22P JPL K154/2	0.54493307 ±9e-8	3.4557183 ±4e-7	4.727895 ±5e-6	120.86178	162.64134	206.26869
30P JPL K103/1	0.5011951 ±2e-7	3.7754076 ±2e-7	8.12265 ±1e-5	119.74115	13.17407	61.00371
78P JPL K114/7	0.46219966 ±9e-8	3.73541262 ±9e-8	6.25491 ±1e-5	210.55664	192.74376	76.36107
115P JPL 16	0.5211645 ±1e-7	4.2597076 ±5e-7	11.687384 ±8e-6	176.50309	120.41045	58.59101
118P JPL 49	0.42817557 ±8e-8	3.4654879 ±2e-7	8.508415 ±5e-6	151.77018	302.17416	143.78902
123P JPL 63	0.4486260 ±1e-7	3.8607445 ±4e-7	15.35692 ±1e-5	46.59827	102.82020	43.33196
157P JPL 28	0.60217 ±1e-5	3.4134 ±1e-4	7.28480 ±7e-5	300.01451	148.84243	174.36079
185P JPL 43	0.6993216 ±1e-7	3.0996991 ±1e-7	14.00701 ±1e-5	214.09101	181.94033	62.38997
Rinner JPL 19	0.39372 ±1e-5	3.79871 ±5e-5	13.77393 ±8e-5	232.01759	221.06138	8.62661
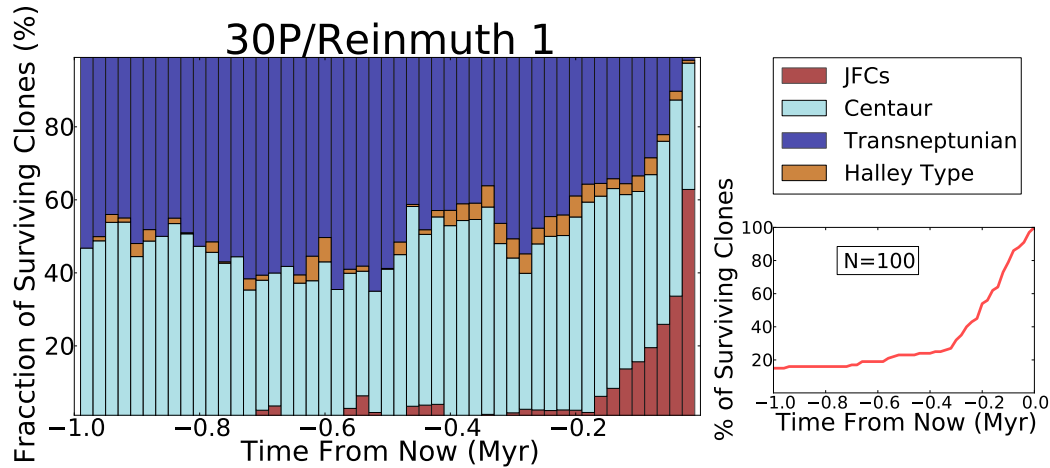
Fig. 20. 30P backward in time orbital evolutionduring 1 Myr. Regions visited by the test particles, and the surviving clones along time. The resolution is 2×10^4 yr.

A special case within the sample is comet 22P, which turned to be the youngest one in our study. Its dynamical analysis shows that the 88% of the test particles are ejected from the Solar System before 1 Myr. The probability to be at the JFCs region in this period remains always under 20% (Fig. 22). If we focused on the last 5×10^3 yr (see Fig. 23) we determine the time spent in JFCs region as ~ 100 yr. This fact is in agreement with its discovery in 1906. It seems that this comet came from the Centaur region, which is the most likely region occupied by the object along this period.
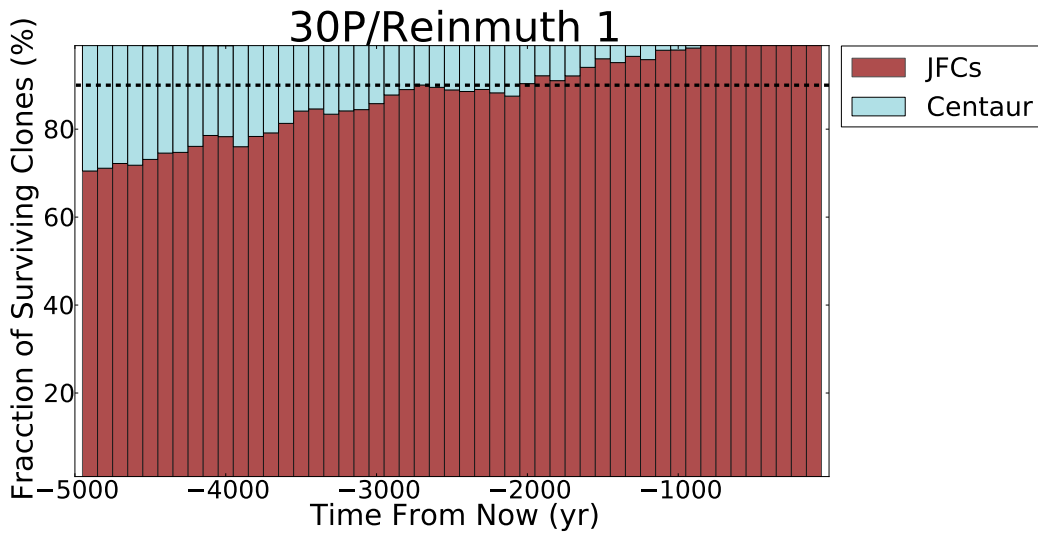
Fig. 21. 30P last $5 \times 10^3 yr$. The dashed line marks the bars with a confidence level equal or larger than 90% of the clones in the Jupiter Family region. The resolution is 100 yr.
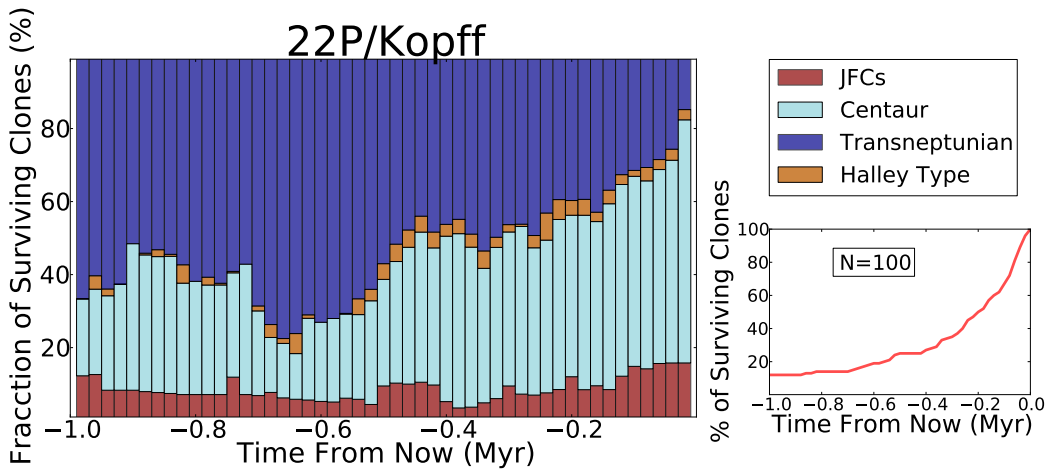

Fig. 22. 22P backward in time orbital evolutionduring 1 Myr. Regions visited by the test particles, and the surviving clones along time. The resolution is 2×10^4 yr.

5.1. Discussion

From the dynamical analysis we obtain that after 15 Myr backward integration, just 12 of the initial 900 particles (9 real comets + 99 clones per each one) survived, what means 1.3%. This result is in agreement with Levison & Duncan (1994), who from their dynamical study concluded that just 11±4 particles, that is $1.5 \pm 0.6\%$, remained in the Solar System after integration. In Fig. 24 we show the surviving clones in the *a-e* plane, where just one of the clones is in the Centaur region (118P/clon74), and the rest of them are in the transneptunian region. Two of the clones have $a > 100$ AU with a very high eccentricity ($e > 0.9$), 30P/clon91 and Rinner/clon31. On the other hand, there are two comets with low eccentricity, 78P/clon86 and 118P/clon13, with $e < 0.25$. The rest of the surviving clones have intermediate values of eccentricity, $0.45 < e < 0.8$, and it seems that these comets are in a transition state between Kuiper Belt and the Scattered Disk objects (Levison & Duncan 1997).
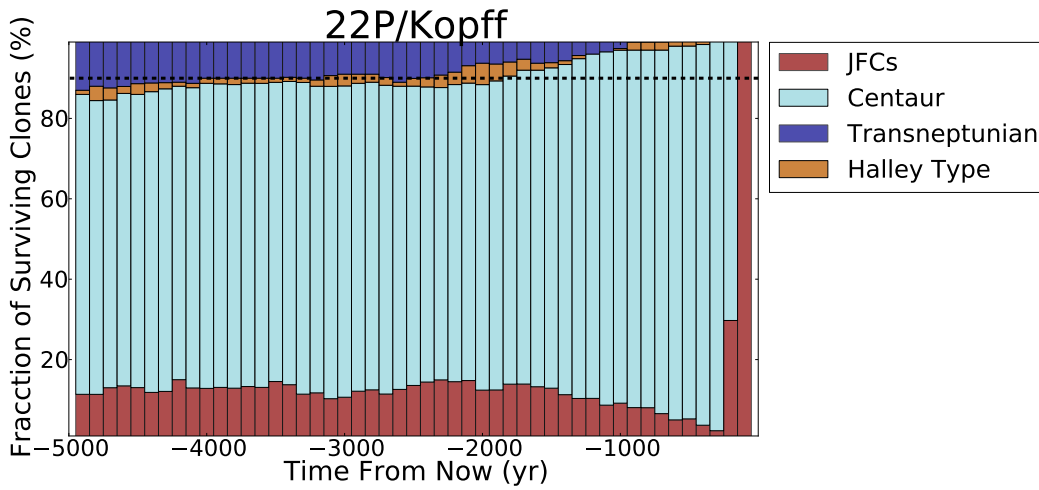
Fig. 23. 22P last $5 \times 10^3 yr$. The dashed line marks the bars with a confidence level equal or larger than 90% of the clones in the Jupiter Family region. The resolution is 100 yr.
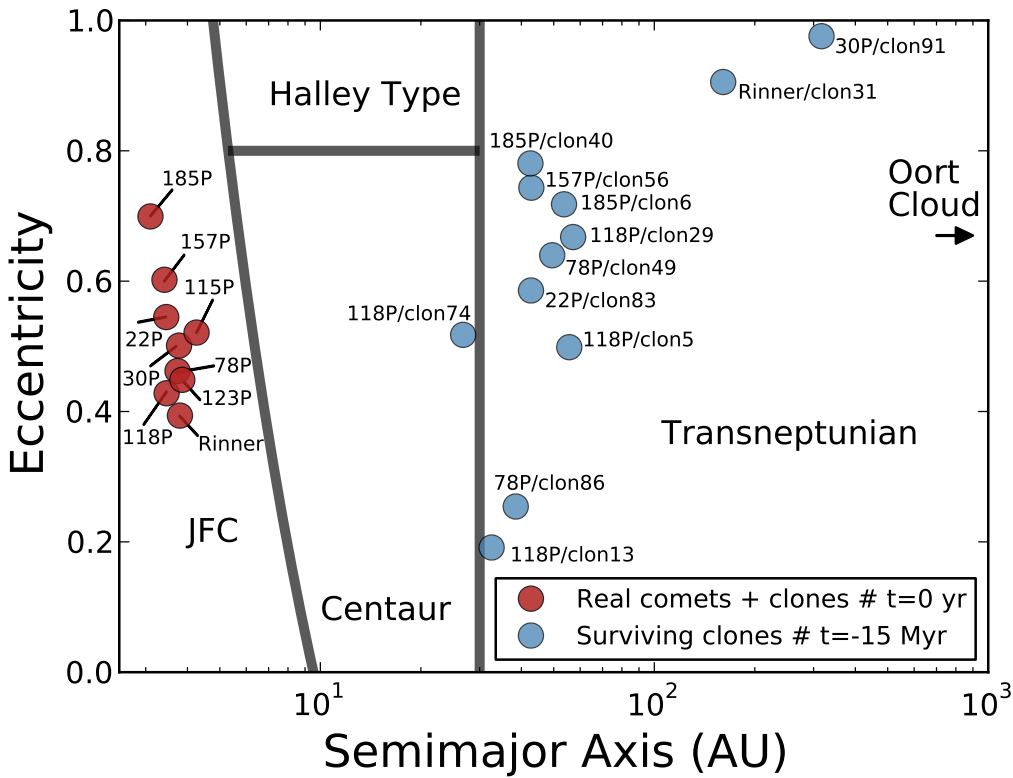

Fig. 24. Time evolution of the 900 initial particles in the 15 Myr backward integration. Red circles are the real comets and their clones (in the same location for t=0 yr, i.e current position, just 2σ dispersion in the orbital parameters), and the blue circles are the surving particles after 15 Myr.

In addition, we derived the time spent by all the comets under study in JFCs region with 90% of confidence level. We can see that the youngest one is 22P, followed by 78P, and 118P ($\sim 100, \sim 500$, and ~ 600 yr respectively). On the other hand, the oldest comet in our sample is 123P, with $\sim 3.9 \times 10^3$ yr. This result is shown in Fig. 25. Finally, if we relate for each comet its annual dust production rate (T_d) within the time spent in the JFCs region, it seems that the most active comet in our sample are at the same time the yougest ones, i.e., 22P, 78P and 118P. This result is shown in Fig. 26
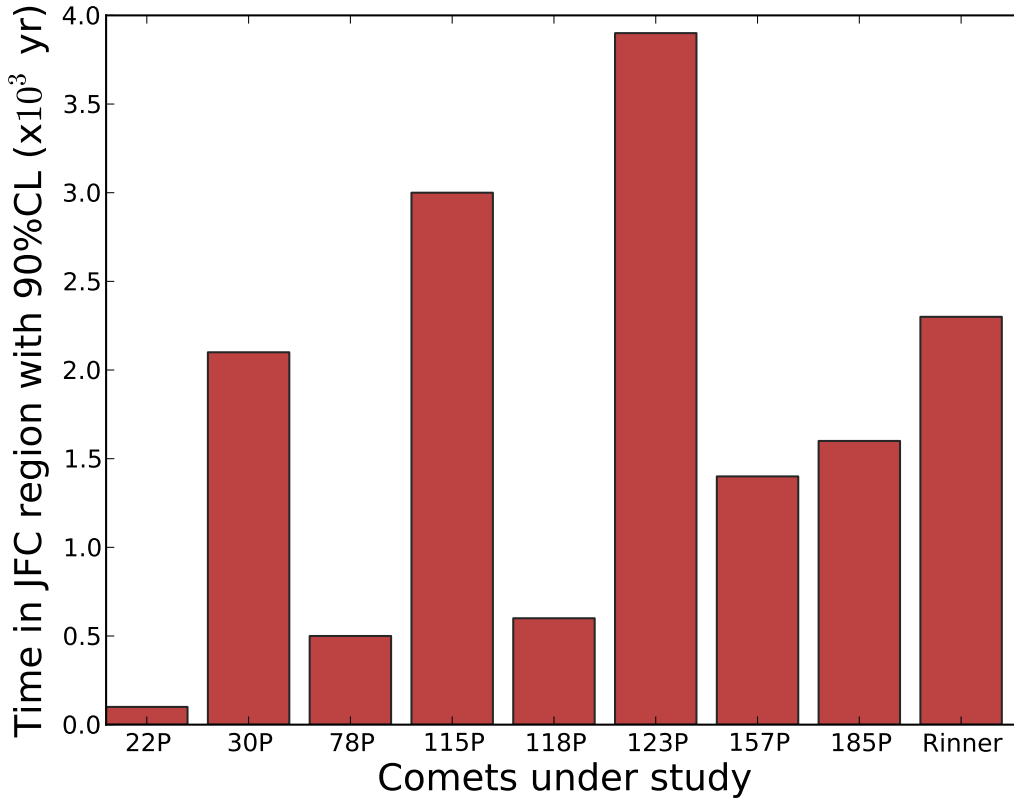
Fig. 25. Time spent by the comets under study in the JFCs region, obtained with a 90% of confidence level.
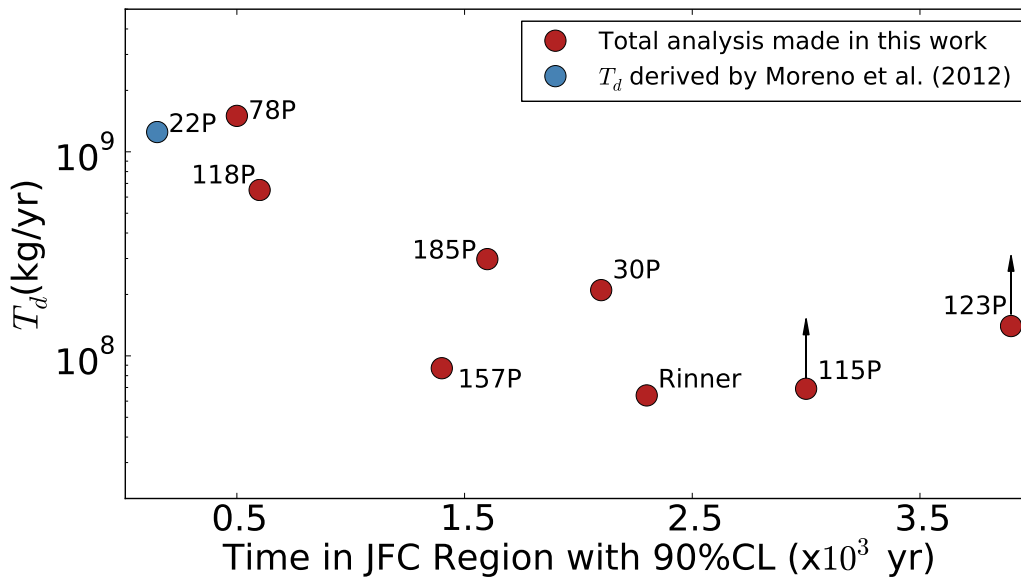

Fig. 26. Annual dust production rate of our targets obtained in the dust analysis (see section 4) versus the time in the JFCs region with a 90%CL derived in dynamical studies (see section 5). The comets with arrows mean the T_d given for them are lower limits.

6. Summmary & Conclusions

1. We present optical observations carried out at Sierra Nevada Observatory 1.52m telescope of eight JFCs comets during their last perihelion passage: 30P/Reinmuth 1, 78P/Gehrels 2, 115P/Maury, 118P/Shoemaker-Levy 4, 123P/West-Hartley, 157P/Tritton, 185/Petriew, and P/2011

W2 (Rinner). Also, we benefited from $Af\rho$ curves of these targets along ~ 300 days around perihelion which is provided by *Cometas-Obs*. We use our Monte Carlo dust tail code (e.g. Moreno 2009) to derive the dust properties of our targets. These properties are: Dust loss rate, ejection velocities of particles, size distribution of particles, where we give the minimum and maximum size of particles and the power index of the size distribution δ. Also we obtain for each comet the overall emission pattern, which can be either isotropic or anisotropic. When the ejection is derived to be anisotropic we can estimate the location of the active areas on the surface and the rotational parameters given by ϕ and I. From this analysis we have determined three categories according to the amount of dust emitted. Weakly active: 115P, 157P, and Rinner with an annual production rate $T_d < 1 \times 10^8$ kg yr^{-1}. Moderately active: 30P, 123P, and 185P with an annual production rate of $T_d = 1 - 3 \times 10^8$ kg yr^{-1}. Highly active: 78P and 118P with values $T_d > 8 \times 10^8$ kg yr^{-1}. In addition to these targets, for our purposes we also took into account the results of the dust characterization given in a previous work by Moreno et al. (2012) for the comet 22P/Kopff. For this object the annual production rate was derived as $T_d = 1.24 \times 10^9$ kg yr^{-1}, what allows us to introduce it in the high emitters category.

2. The second part of our study was the determination of the dynamical evolution followed by the comets of the sample in the last 1 Myr. With this purpose we use the numerical integrator develop by Chambers (1999). In this case we neglected the non gravitational forces due to the little contribution of a single jet in the motion of our targets. We derived its maximum influence over a as 0.21 AU during the lifetime of the sublimation jet. In order to make a statistical study of the dynamical evolution we used 99 clones with 2σ dispersion in the orbital parameters (a, e, and i), plus the real one. So we had 100 test particles to determine which were the most visited regions by each comet and when. This analysis allowed us to determinate how long spent these comets as members of JFCs, region of special interest because it is supposed that it is in this place where the comets became active sublimating the ices trapped in the nucleus which belong to the primitive chemical components of the Solar System when was formed. From the dynamical study we inferred that our targets are relatively young in the JFC region, with ages between $100 < t < 4000$ years and all of them have a Centaur and Transneptunian past, as expected.

3. The last point in our conclusions lead us to relate the results in the previous points. In Fig. 26 we plot each comet attending to the averaged dust production rate [kg/yr] derived in the dust characterizations (see table 4 in section 4) and the time spent in the JFCs region obtained in the dynamical analysis (see Fig. 25 in section 5). Attending to this figure we conclude that the most active comets in our target list are at the same time the youngest ones (22P, 78P, and 118P). However, although the other targets show a similar trend in general, there are some exceptions (e.g., 157P and 123P) that prevent us from reaching a firm conclusion. A more extended study of this kind would be then desirable.

References

A'Hearn, M. F., Belton, M. J. S., Delamere, W. A., et al. 2005, Science, 310, 258

A'Hearn, M. F., Schleicher, D. G., Millis, R. L., Feldman, P. D., & Thompson, D. T. 1984, AJ, 89, 579

Brownlee, D. E., Horz, F., Newburn, R. L., et al. 2004, Science, 304, 1764

Burns, J. A., Lamy, P. L., & Soter, S. 1979, Icarus, 40, 1

Carry, B. 2012, Planet. Space Sci., 73, 98

Chambers, J. E. 1999, MNRAS, 304, 793

Davidsson, B. J. R. & Gutierrez, P. J. 2004, in Bulletin of the American Astronomical Society, Vol. 36, AAS/Division for Planetary Sciences Meeting Abstracts #36, 1118

Duncan, M., Levison, H., & Dones, L. 2004, Dynamical evolution of ecliptic comets, ed. M. C. Festou, H. U. Keller, & H. A. Weaver, 193–204

Edoh, O. 1983, Univ. Arizona

Finson, M. J. & Probstein, R. F. 1968, ApJ, 154, 327

Fulle, M., Colangeli, L., Agarwal, J., et al. 2010, A&A, 522, A63

Grun, E., Zook, H. A., Fechtig, H., & Giese, R. H. 1985, Icarus, 62, 244

Hartogh, P., Lis, D. C., Bockelée-Morvan, D., et al. 2011, Nature, 478, 218

Hsieh, H. H., Yang, B., & Haghighipour, N. 2012a, ApJ, 744, 9

Hsieh, H. H., Yang, B., Haghighipour, N., et al. 2012b, AJ, 143, 104

Jewitt, D. 2009, AJ, 137, 4296

Jockers, K. 1997, Earth Moon and Planets, 79, 221

Keller, H. U., Arpigny, C., Barbieri, C., et al. 1986, Nature, 321, 320

Kolokolova, L., Hanner, M. S., Levasseur-Regourd, A.-C., & Gustafson, B. Å. S. 2004, Physical properties of cometary dust from light scattering and thermal emission, ed. G. W. Kronk, 577–604

Krolikowska, M., Sitarski, G., & Szutowicz, S. 1998, Acta Astron., 48, 91

Lacerda, P. 2013, MNRAS, 428, 1818

Lamy, P. L., Toth, I., Fernandez, Y. R., & Weaver, H. A. 2004, The sizes, shapes, albedos, and colors of cometary nuclei, ed. G. W. Kronk, 223–264

Levison, H. F. & Duncan, M. J. 1994, Icarus, 108, 18

Levison, H. F. & Duncan, M. J. 1997, Icarus, 127, 13

Lowry, S. C. & Weissman, P. R. 2003, Icarus, 164, 492

Mazzotta Epifani, E. & Palumbo, P. 2011, A&A, 525, A62

Meech, K. J. & Jewitt, D. C. 1987, A&A, 187, 585

Monet, D. G., Levine, S. E., Canzian, B., et al. 2003, AJ, 125, 984

Moreno, F. 2009, ApJS, 183, 33

Moreno, F., Lara, L. M., Licandro, J., et al. 2011, ApJ, 738, L16

Moreno, F., Pozuelos, F., Aceituno, F., et al. 2012, ApJ, 752, 136

Schwehm, G. & Schulz, R. 1998, in Astrophysics and Space Science Library, Vol. 236, Laboratory astrophysics and space research, ed. P. Ehrenfreund, C. Krafft, H. Kochan, & V. Pirronello, 537

Scotti, J. V. 1994, in Bulletin of the American Astronomical Society, Vol. 26, American Astronomical Society Meeting Abstracts, 1375

Sekanina, Z. 1981, Annual Review of Earth and Planetary Sciences, 9, 113

Soderblom, L. A., Becker, T. L., Bennett, G., et al. 2002, Science, 296, 1087

Sykes, M. V., Grün, E., Reach, W. T., & Jenniskens, P. 2004, The interplanetary dust complex and comets, ed. M. C. Festou, H. U. Keller, & H. A. Weaver, 677–693

Tancredi, G., Fernández, J. A., Rickman, H., & Licandro, J. 2006, Icarus, 182, 527

List of Objects

Table 3. Dust properties summary of the targets under study I

Comet	Emission pattern [1]	Active areas location (°)	Size distribution r_{min}, r_{max} (cm)	Size distribution $\delta_{min}, \delta_{max}$	Maximum nucleus radius (km)	Obliquity (°)	Argument of subsolar meridan at perihelion (°)
30P/Reinmuth 1	Ani (50%)	-30 to +30	10^{-4}, 3.5	-3.35, -3.18	3.9 [2]	107 [3]	133 [3]
78P/Gehrels 2	Iso (100%)	–	10^{-4}, 3.0	-3.40, -3.05	3.6	–	–
115P/Maury	Ani (70%)	-20 to +60	10^{-4}, 4.0	-3.13, -3.05	4.0	25	280
118P/Shoemaker-Levy 4	Iso (100%)	–	10^{-4}, 3.0	-3.20, -3.05	2.4 [4]	–	–
123P/West-Hartley	Iso (100%)	–	10^{-4}, 2.5	-3.32, -3.15	2.0 [5]	–	–
157P/Tritton	Ani (70%)	-30 to +30	10^{-4}, 3.0	-3.35, -3.15	1.6	10	150
185P/Petriew	Iso (100%)	–	10^{-4}, 6.0	-3.60, -3.00	5.7	–	–
P/2011 W2 (Rinner)	Iso (100%)	–	10^{-4}, 2.5	-3.20, -3.15	2.2	–	–

Notes.

[1] Iso=Isontropic ejection; Ani=Anisotropic ejection.

[2] Scotti (1994)

[3] Krolikowska et al. (1998)

[4] Lamy et al. (2004)

[5] Tancredi et al. (2006)

Table 4. Dust properties summary of the targets under study II

Comet	Peak dust loss rate (kg/s)	Peak ejection velocity of 1-cm grains (m/s)	Total dust mass ejected (kg)	Total dust mass ejected per year (kg/yr)	Averaged dust mass loss rate (kg/s)	Contribution to the interplanetary dust (%) [1]
30P/Reinmuth 1	73.0	1.4	8.2×10^8	2.1×10^8	6.8	0.07
78P/Gehrels 2	530.0	2.1	5.8×10^9	1.5×10^9	47.5	0.52
115P/Maury	45.0	1.4	2.9×10^8	6.9×10^7	2.1	0.02
118P/Shoemaker-Levy 4	180.0	2.3	2.3×10^9	6.5×10^8	20.8	0.22
123P/West-Hartley	65.0	1.8	5.4×10^8	1.4×10^8	4.5	0.05
157P/Tritton	50.0	2.1	2.9×10^8	8.7×10^7	2.7	0.03
185P/Petriew	143.0	7.2	9.0×10^8	3.0×10^8	9.6	0.10
P/2011 W2 (Rinner)	15.0	1.7	2.6×10^8	6.4×10^7	2.0	0.02

Notes.

[1] Annual contribution to the interplanetary dust replacement (Grun et al. 1985).